ATLAS Note

GROUP-2017-XX

11th December 2019

Draft version 0.1

Combination of ATLAS and Tevatron W boson mass measurements

The ATLAS, CDF and D0 Collaborations

This note presents a combination of the ATLAS, CDF and D0 measurements of the W-boson mass. These measurements were performed at different moments in time, using different modelling assumptions for W-boson production and decay, using fits to detector-level distributions. The correlations between these measurements are dominated by uncertainties in the PDFs, for which different choices were made. Methods are presented to evaluate the effect of PDF variations on existing measurement results in a realistic way, which allows extrapolating past measurements to any past or present PDF set and eevaluate the corresponding uncertainties. Based on this method, the measurements can be corrected to set of common PDF references, and combined accounting for PDF correlations in a rigourous way. The combined value is

$$m_W = 80XYZ \pm X(\text{exp.}) \pm Y(\text{PDF}) \pm Z(\text{mod.})$$

where the central value has been obtained for PDF set to be defined. The quoted PDF uncertainty includes the effect of partial correlations between the experiments. Central values for alternate sets are also given.

Contents

TO DO

- improve (rebin) pTZ constraint plots
- compare PDF uncertainties with showered and unshowered evgen
- add CTEQ6.1 PDF uncertainties to D0 result
- improve D0 parameterisation

1 Introduction

The present note describes a combination of the CDF [1], D0 [2] and ATLAS [3] measurements of the W-boson mass, m_W. At hadron colliders, measurements of m_W rely on the interpretation of the kinematic peaks in leptonic decays. The final-state distributions carry information about the decaying particle mass, but also reflect the W production distributions, in particular the rapidity and transverse momentum distributions, and polarization. Predictions for the latter are obtained using event generators and parton distribution functions (PDFs) that are state-of-the-art at the time the measurements are performed, and typically differ between measurements.

The Tevatron and LHC measurements discussed here were performed at distant moments in time, and used different tools for the theoretical description of W-boson production and decay. Specifically, CDF and D0 used the ResBos [4–6] event generator for the prediction of the p_T^W distribution and the CTEQ6.6 PDF set [7], and ATLAS used Powheg [8–10], Pythia [11] and CT10 [12]. Combining both sets of results thus involves three steps : first, translate both results to a common reference model, *i.e.* a common set of proton PDFs; secondly, evaluate the correlation of PDF uncertainties at the Tevatron and LHC – while both machines are hadron colliders, the different center-of-mass energies (2 and 7 TeV for the Tevatron and LHC measurements, respectively) and initial states ($p\bar{p}$ vs. pp) makes this correlation non-trivial; finally, evaluate the model dependence of the result by repeating this procedure for a relevant set of current PDF sets.

A proper evaluation of PDF uncertainties and their correlations is numerically relevant, as PDFs constitute the dominant source of uncertainty for all measurements. While significant in size, uncertainties related to the p_T^W distribution are evaluated separately in each experiment through a detailed analysis of Z-boson production *in situ*, reducing correlations across experiments. Experimental uncertainties are by nature uncorrelated.

Beyond the interest of improving the overall measurement precision, several arguments motivate this project :

- At least three private, semi-qualitative averages are being used in recent literature [13–15]. While these numbers are probably numerically close to the actual result, they do not rely on a well established methodology that can be used for future averages of this or other hadron collider parameters, and neglect the fact that the measurements were performed assuming different PDF sets;
- the techniques developed to translate published measurements to a common PDF reference can also be used to update measurements to newer, more precise PDF sets;
- PDF uncertainty correlations, discussed here for the first time in the context of electroweak precision measurements, will also matter in the joint interpretation of different parameters in electroweak or EFT fits. For example, strong PDF uncertainty correlations are expected between m_W and the effective weak mixing angle, $\sin^2\theta_{\text{eff}}$, when the LHC ultimately dominates the measurement precision for these parameters.

A general discussion of uncertainty correlations in m_W measurements is first given in Section 2. Sections 3 and 4 describe the general analysis methodology and the event samples used for the present analysis; analysis details are described in Section 5. Section 6.1–6.3 present extrapolations of the published CDF, D0 and ATLAS measurements to different PDF sets. Section 6.4 presents the fully combined results and gives PDF uncertainty correlations across experiments; finally, conclusions are given in Section 7.

2 Correlated and uncorrelated sources of uncertainty

Experimental uncertainties are by nature uncorrelated across experiments. Modelling uncertainties can be categorized as induced by the PDFs, by the p_{T}^{W} distributions or by electroweak corrections and are discussed below.

2.1 Electroweak corrections

The dominant effect of QED radiation on the W boson mass measurement is the reduction of the measured lepton momentum due to final-state radiation. The experiments model this radiation with the PHOTOS generator that produces a shower of photons above an energy threshold. Uncertainties on the modelling of electroweak corrections include: (1) the difference between the shower model and an explicit matrix-element calculation; (2) the energy threshold for producing final-state photons; and (3) higher-order corrections from final-state e^+e^- pair production. Tables 1 and 2 list these uncertainties for each experiment in the electron and muon channels, respectively. The uncertainties are completely correlated between the channels.

Uncertainty	CDF	D0	ATLAS	CDF-ATLAS	CDF-D0	D0-ATLAS
NLO calculation	4 (4)	5 (5)	2.5 (3.3)	0%	0%	100%
Photon y cutoff	2 (2)	2 (1)	−−	−−	100%	−−
FSR e^+e^-	1 (1)	−−	0.8 (3.6)	0%	−−	−−
Total	4 (4)	7 (7)	2.6 (4.9)			

Table 1: QED uncertainties in MeV on the m_W measurement in the electron channel using the m_T (p_T) fit. Uncertainty correlations between each pair of experiments are shown.

Uncertainty	CDF	ATLAS
NLO calculation	4 (4)	2.5 (3.5)
Photon y cutoff	2 (2)	−−
FSR e^+e^-	1 (1)	0.8 (3.6)
Total	4 (4)	2.6 (5.6)

Table 2: QED uncertainties in MeV on the m_W measurement in the muon channel using the m_T (p_T) fit. The uncertainties are uncorrelated between the experiments.

To estimate the uncertainty from the limitations of the shower model relative to the matrix-element calculation, D0 performs a direct comparison between PHOTOS and WGRAD. ATLAS estimates the uncertainty with a similar procedure but with WINHAC providing the NLO model. The uncertainties are taken to be completely correlated between these experiments. CDF uses a different strategy, applying a correction to the measurement using the HORACE generator, which matches single-photon radiation to the NLO calculation. The residual uncertainty is entirely due to MC statistics, and is uncorrelated with the D0 and ATLAS uncertainties.

The shower model includes a lower threshold on the photon energy, expressed as a ratio y with respect to the energy of the lepton from the W boson decay. CDF uses a threshold of 10^{-5} and determines the uncertainty by increasing the threshold by an order of magnitude. D0 uses a similar procedure except with an increase from 2.5×10^{-4} to 2×10^{-2} in y. These uncertainties are taken to be completely correlated.

To account for the higher-order process of an off-shell final-state photon splitting into an e^+e^- pair, CDF applies an effective radiator approximation to the radiated photons. ATLAS does not apply a correction, instead taking the uncertainty from a PHOTOS model of this process. The uncertainties are treated as uncorrelated.

2.2 W-boson p_{T} distribution

The prediction of the W-boson p_{T} distribution is a second potential source of uncertainty correlation. In the region relevant for m_W, the p_{T} distribution is described by a combination of perturbative fixed-order QCD, soft-gluon resummation and non-perturbative effects. The Tevatron experiments rely on analytical resummation as implemented in ResBos, while ATLAS used the Pythia parton shower.

Non-perturbative effects influence the very low boson p_{T}^W region, typically $p_{\mathrm{T}}^W < 5$ GeV and are generally assumed universal between W and Z production. In absence of precise direct measurements of the W-boson p_{T} distribution, all measurements rely on Z-boson data to constrain the corresponding parameters.

The resulting model is then used for the prediction of the W-boson p_{T} distribution. The associated uncertainty originates from the limited precision of the Z-boson data, and from differences between the Z and W production mechanisms, in particular related to the different initial-state partonic configurations.

ATLAS, CDF and D0 derive the W-boson production model from their respective Z-boson data. Uncertainties from parton-level differences between Z and W production are only considered in ATLAS. Uncertainties related to the W-boson p_{T} distribution can thus be considered as uncorrelated between the three experiments.

2.3 PDF uncertainties

PDF uncertainties constitute the main source of correlation between the measurements. In the case of the Tevatron-only combination [16], the very similar measurement conditions implied full correlation of the PDF uncertainty, considered as a single nuisance parameter. In contrast, the large gap in energy between the Tevatron and the LHC, as well the different initial states are expected to induce only a partial correlation of these uncertainties, and a detailed study of the PDF uncertainty components is required. Methods to estimate this correlation are described in Section 3.

3 General methodology

3.1 Overview

The proposed method relies on an emulation of the existing measurements. The emulation consists of simplified parameterizations of the response of the experiments, and a reproduction of the corresponding analyses (event selections, fitting procedure, etc). While this approach is obviously not adequate for an actual measurement, it is sufficient for a reliable estimation of PDF uncertainties, as shown in Section 3.2. The emulation of the ATLAS, CDF and D0 measurements in described in Sections 6.1–6.3.

This emulation is applied to particle-level W- and Z-event samples that include event weights allowing to reproduce the production and decay distributions expected for an ensemble of PDF sets, including those used for the published measurements and a choice of more recent sets. The initial states reproduce the measurement conditions, ie $p\bar{p}$ collisions at 2 TeV for the Tevatron, and pp collisions at 7 TeV for ATLAS. Full details are given in Section 4.

The Monte Carlo samples are produced using a reference value for the W-boson mass and the corresponding Standard Model prediction for Γ_W. Kinematic distributions for different values of m_W are obtained by applying the following event weight:

$$w(m, m_W, m_W^{\mathrm{ref}}) = \frac{(m^2 - m_W^2)^2 + m^4\Gamma_w^2/m_W^2}{(m^2 - m_W^{\mathrm{ref}2})^2 + m^4\Gamma_w^2/m_W^{\mathrm{ref}2}} \quad (1)$$

which represents the ratio of the Breit–Wigner densities corresponding to m_W and m_W^{ref}, for a given value of the final state invariant mass m.

The shift in the measured value of m_W resulting from a change in the assumed PDF set is estimated as follows. Considering a set of template distributions obtained for different values of m_W and a given reference PDF set, and "pseudo-data" distributions obtained for $m_W = m_W^{\mathrm{ref}}$ and an alternate set i (representing the difference between the nominal predictions of two PDF sets, or uncertainty variations with respect to a given nominal PDF set), the preferred value of m_W for this set is determined by minimizing the χ^2 between the pseudo-data and the templates. The preferred value of m_W for this set is denoted m_W^i, and the corresponding shift is defined as $\delta m_W^i = m_W^i - m_W^{\mathrm{ref}}$.

The shifts are used to extrapolate existing measurements to alternate PDF sets and to estimate the corresponding PDF uncertainty, as discussed in Section 3.2. The procedure is validated by comparing the obtained PDF uncertainties with the published numbers.

For a proper evaluation of the PDF uncertainty correlations, the latter need to be evaluated for all existing measurement channels or categories, and combined. This includes six measurements for CDF (with fits to the p_{T}^{ℓ}, m_{T} and $E_{\mathrm{T}}^{\mathrm{miss}}$ distributions in the $W \to e\nu, \mu\nu$ channels); two measurements for D0 (fits to the p_{T}^{ℓ} and m_{T} distributions in the $W \to e\nu$ channel), and 28 measurement categories for ATLAS (with fits to the p_{T}^{ℓ} and m_{T} distributions in the $W \to e\nu$, and $W \to \mu\nu$ channels, with three and four pseudorapidity categories respectively, separately for W^+ and W^- events). Combinations are performed using the BLUE method [17], as was used in all published measurements. Partial combinations, *i.e* reproducing published numbers for the individual CDF, D0 and ATLAS combinations and for the Tevatron combination provides further validation. Finally, a complete combination can be performed.

This procedure is repeated for a representative ensemble of current PDF sets, to evaluate the model dependence of the PDF correlations. The combined values of m_W are then compared for various PDF sets, and final prescription is given to define the reference combined value.

3.2 Impact of PDF variations on measurements of m_W

Correcting existing measurements to alternate PDFs

Denoting $m_W^{\mathrm{data}\,|\,\mathrm{ref}}$ the result of a measurement performed using a reference PDF set, and $m_W^{\mathrm{data}\,|\,\mathrm{alt}}$ the result corrected to an alternate PDF set, the latter can be written

$$m_W^{\mathrm{data}\,|\,\mathrm{alt}} = m_W^{\mathrm{data}\,|\,\mathrm{ref}} - \delta m_W^{\mathrm{alt}} \quad (2)$$

where δm_W is introduced in the previous section and defined with respect to the reference PDF set. Published values are always used for $m_W^{\text{data}\,|\,\text{ref}}$; the measurement emulation procedure is only used for δm_W^{alt}.

PDF uncertainties

For Hessian PDF sets, the uncertainty corresponding to a given set is estimated as

$$\delta m_W^+ = \left[\sum_i \left(\delta m_W^i\right)^2\right]^{1/2} \text{ if } \delta m_W^i > 0, \qquad \delta m_W^- = \left[\sum_i \left(\delta m_W^i\right)^2\right]^{1/2} \text{ if } \delta m_W^i < 0, \tag{3}$$

where i runs over the uncertainty sets, and δm_W^i is the difference between the fitted value for set i and the reference PDF set. Only symmetrized uncertainties, $\delta m_W = (\delta m_W^+ + \delta m_W^-)/2$, are discussed below for simplicity.

The effect of each PDF eigenset is fully correlated across experiment or measurement categories, and its contribution to the covariance between any two measurements α, β is given by

$$C^i_{\alpha\beta} = \delta m^i_{W\alpha} \delta m^i_{W\beta}. \tag{4}$$

Accounting for all eigensets of a given set, the total PDF uncertainty covariance and the corresponding uncertainty correlation are calculated as

$$C^{\text{PDF}}_{\alpha\beta} = \sum_i C^i_{\alpha\beta}, \tag{5}$$

$$\rho_{\alpha\beta} = \frac{\sum_i \delta m^i_{W\alpha} \delta m^i_{W\beta}}{\delta m_{W\alpha} \delta m_{W\beta}}. \tag{6}$$

In the case of NNPDF, which provides PDF replica sets from fits to fluctuated data, the uncertainty is estimated from the spread of the fitted values of m_W over the N replicas:

$$\delta m_W = \left[\frac{1}{N} \sum_i \left(\delta m_W^i\right)^2\right]^{1/2}. \tag{7}$$

ATLAS case : p_{T}^Z-constrained PDF uncertainties

Due do their influence on the rate of W, Z-boson production in association with jets, PDFs contribute to the uncertainty in the vector boson p_{T} distributions. The ATLAS measurement accounts for the precisely measured Z-boson p_{T} distribution at 7 TeV [18] by correcting the PDF weight returned by Powheg as follows:

$$w^{\text{corr}}_{i\to j} \equiv w_{i\to j} \times \left(\frac{1}{\sigma_Z}\frac{d\sigma_Z}{dp_{\text{T}}}\right)_i \bigg/ \left(\frac{1}{\sigma_Z}\frac{d\sigma_Z}{dp_{\text{T}}}\right)_j \tag{8}$$

where $w_{i\to j}$ is the Powheg PDF weight modifying the generated distributions from PDF sets i and j. This correction ensures that the Z-boson p_{T} distribution remains unchanged, and removes the part of the corresponding W-boson uncertainty that is correlated to the Z. This is approximately equivalent to re-tuning the Pythia parton shower to the Z data for each PDF variation, but simpler in practice. The impact of this correcting weight on the generator-level W^+- and W^--boson p_{T} distribution at 7 TeV is illustrated in Figure 1 for CT10; the effect on the transverse mass and lepton p_{T} distributions is shown in Figure 2. Other PDFs are illustrated in Figure 11 in Appendix A.

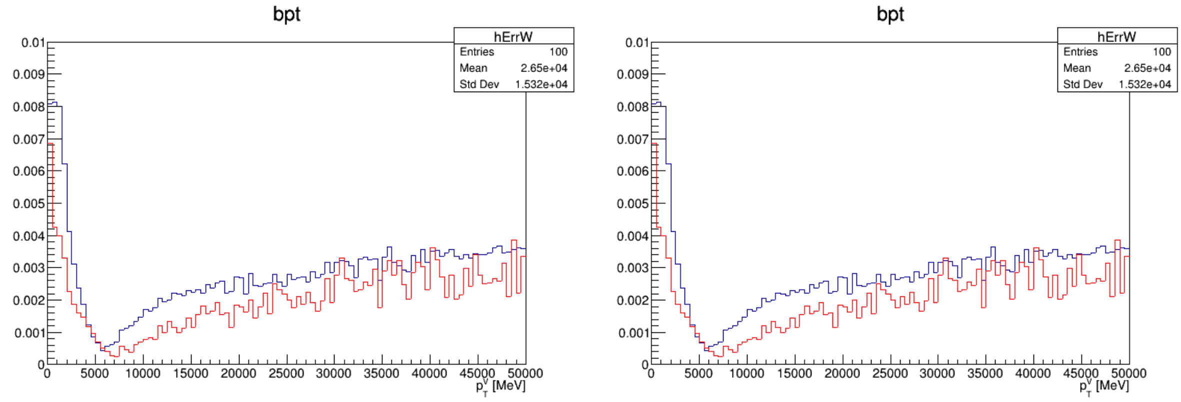

Figure 1: Effect of the pTZ constraint on the generator-level W^+- and W^--boson p_{T} distributions. The blue and red curves represent the conventional and p_{T}^{Z}-constrained PDF uncertainties, respectively.

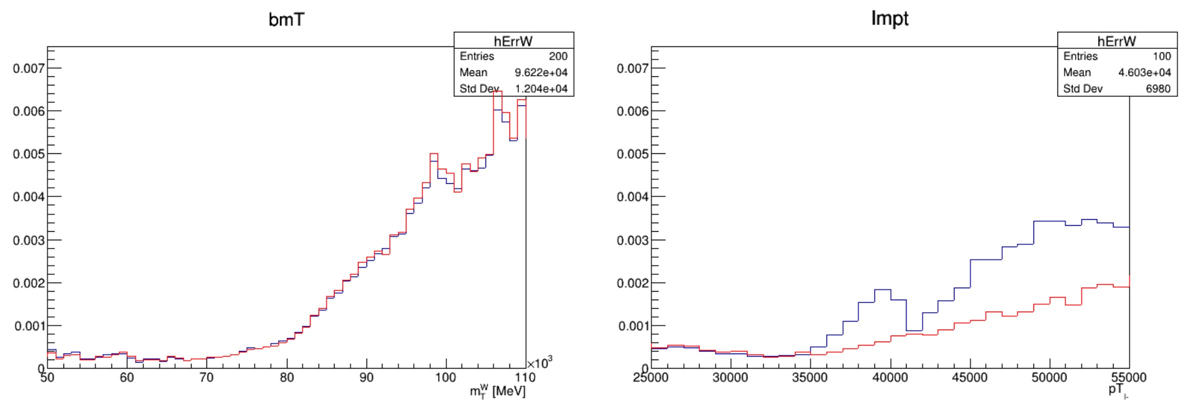

Figure 2: Effect of the pTZ constraint on the generator-level transverse mass and lepton p_{T} distributions. The blue and red curves represent the conventional and p_{T}^{Z}-constrained PDF uncertainties, respectively. The p_{T}^{Z}-constraint significantly reduces the uncertainty in the p_{T}^{ℓ} distribution as expected; the m_{T} distribution, which is by construction insensitive to p_{T}^{W} modelling uncertainties, is mostly unaffected.

4 Event generation

The generation of $W \to \ell\nu$ and $Z \to \ell\ell$ events both for pp collisions at $\sqrt{s} = 7$ TeV and $p\bar{p}$ colissions at $\sqrt{s} = 1.96$ TeV relies on the Powheg V2 event generator [8–10]. The W_ew_BMNNP [19] and Z_ew_BMNNPV [20] processes are used without the NLO electroweak corrections. Final-state QED corrections (QED FSR) are applied using Photos [21].

Apart from the collinear photon radiation, which can be completely absorbed by "dressing" the leptons with all QED FSR photons within a cone of $\Delta R < 0.1$ around the final state lepton, the generated electron and muon decays are identical. It is sufficient to generate just the muon decays.

The nominal event generation is performed with the CT10 PDF set [12]. Weights are calculated internally by Powheg that allow the samples to be reweighted to several alternate PDF sets including their eigenvectors or replicas to estimate the effects of PDF uncertainties and their correlations: CT10 [12], CTEQ6.1 [22] [1], CTEQ6.6 [7], CT10nnlo [23], CT14nnlo [24], CT18NNLO and CT18ANNLO [25], MSTW2008nlo with both the 68% CL and 90% CL error sets [26], MMHT2014nnlo 68%CL [27], NNPDF31_nnlo_as_0118 [28], ABMP16_5_nnlo [29] and CJ15nlo [30].

A first set of samples was produced interfacing Powheg to the Pythia 8 event generator [11] with parameters set according to the AZNLO tune [31]. This gives the best-possible modelling of the full final state, including the effects from parton showering, intrinsic k_{T} and underlying event. Although the computing requirements of these types of samples are still modest, it involves three steps with two large intermediate output formats to arrive at the final analysis ntuple: first EVNT files are produced from the Powheg+Pythia 8+Photos stage; EVNT files are converted to Truth DAOD format; finally TruthDAOD are processed with the MiniTree maker to ntuple format.

However, eventually only the four-vectors of leptons ($\ell^{\pm}, \nu$) at bare and dressed QED level are required for the analysis. A more efficient way with minimal loss of accuracy was therefore chosen to generate the samples: Powheg LHE events are directly interfaced to Photos, an empirical "shower" algorithm is applied to smear the transverse momentum while respecting the leading p_{T} emission already generated by Powheg, and finally the events are directly written to disk in the form of the small analysis ntuple. This processing chain requires just a single step and no intermediate files need to be written to disk. [2]

5 Measurement emulation

5.1 Parameterisation of the ATLAS, CDF and D0 experimental resolutions

ATLAS, CDF and D0 use different notations and conventions to parameterise the recoil response and resolution. Introducing $u_{\parallel}$ and $u_{\perp}$, the projections of the recoil on the axes parallel and perpendicular to the W boson line of flight, we compare the experiments in terms of a response function $R \equiv -\left\langle u_{\parallel} \right\rangle / p_{\mathrm{T}}^{W}$, and resolution functions $\sigma_{u_{\parallel}}$ and $\sigma_{u_{\perp}}$. R represents the ratio between the reconstructed and true transverse momentum of the W boson; the resolution of $u_{\parallel}$, $\sigma_{u_{\parallel}}$, is expected to be slightly larger than $\sigma_{u_{\perp}}$ due to the presence of hard radiation recoiling against the W.

Resolution effects in lepton reconstruction are also accounted for in the procedure. With a typical relative momentum resolution of about 2% for all experiments, these effects are subleading and not discussed further.

[1] Special thanks to Andy Buckley for converting the PDF set from LHAPDF5 to LHAPDF6 version.
[2] If necessary, events can still be reweighted to the Powheg+Pythia8 AZNLO prediction of vector boson p_{T}.

The recoil response functions for CDF are parameterised in terms of the recoil magnitude and angular resolution. For $p_{\mathrm{T}}^{W} < p_{\mathrm{T}}^{\max} = 15$ GeV:

$$
\begin{aligned}
R(p_{\mathrm{T}}^{W}) &= 0.645 \times \log(5.1 \times p_{\mathrm{T}}^{W} + 8.2)/\log(5.1 \times p_{\mathrm{T}}^{\max} + 8.2), && (9)\\
\sigma_{u_{\mathrm{T}}}(p_{\mathrm{T}}^{W}) &= 0.82 \times \sqrt{p_{\mathrm{T}}^{W}}\ \text{GeV}, && (10)\\
\sigma_{u_{\phi}}(p_{\mathrm{T}}^{W}) &= 0.306 + 0.021 \times (9.4 - p_{\mathrm{T}}^{W})\ \text{rad}; && (11)
\end{aligned}
$$

while for $p_{\mathrm{T}}^{W} > p_{\mathrm{T}}^{\max}$ the angular resolution becomes

$$
\sigma_{u_{\phi}}(p_{\mathrm{T}}^{W}) = 0.144 + 0.0048 \times (24.5 - p_{\mathrm{T}}^{W})\ \text{rad}. \qquad (12)
$$

A simplified parameterisation of the recoil response for D0, adequate for the purpose of this study, is[3]:

$$
\begin{aligned}
R(p_{\mathrm{T}}^{W}) &= 0.46/p_{\mathrm{T}}^{W} - 0.55 - 0.0021 \times p_{\mathrm{T}}^{W}, && (13)\\
\sigma_{u_{\perp}}(p_{\mathrm{T}}^{W}) &= 3.6 + 0.013 \times p_{\mathrm{T}}^{W} + 0.00010 \times p_{\mathrm{T}}^{W\,2}\ \text{GeV}, && (14)\\
\sigma_{u_{\parallel}}(p_{\mathrm{T}}^{W}) &= 3.5 - 0.055 \times p_{\mathrm{T}}^{W} + 0.00072 \times p_{\mathrm{T}}^{W\,2}\ \text{GeV}. && (15)
\end{aligned}
$$

Both experiments achieve a typical resolution of 4–5 GeV in the p_{T}^{W} range relevant for the measurement.

For ATLAS, the recoil response is extracted from profiles of R, $\sigma_{u_{\parallel}}$ and $\sigma_{u_{\perp}}$ as a function of the W-boson transverse momentum, obtained from the simulation and corrected for calibration discrepancies. The recoil resolution is about 12–16 GeV, mostly depending on the amount of pile-up.

The performances of ATLAS, CDF and D0 for the recoil response are compared in Figure 3.

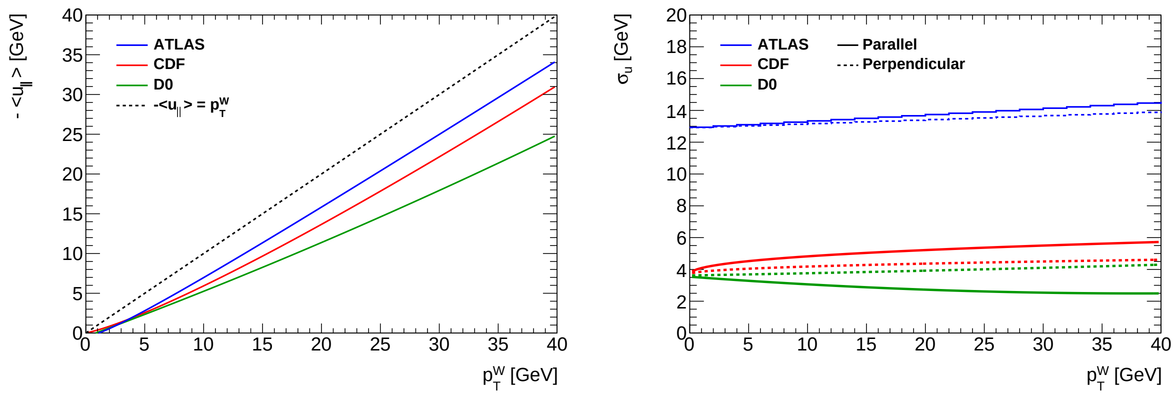

Figure 3: Comparison of the parameterised recoil response (left) and resolution (right) for ATLAS, CDF and D0.

5.2 Event selections, fit ranges and measurement categories

Event selections and fitting ranges for the three measurements are summarized in Table 3. CDF and D0 use very similar analysis configurations. The looser recoil cut and wider m_{T} fit range in ATLAS are a consequence of the worse recoil resolution. The multijet background is enhanced in ATLAS due to the worse recoil resolution and the higher collision energy; the tighter p_{T}^{ℓ} fit range mitigates this effect.

[3] R. Coelho Lopes de Sa, private communication.

Experiment	Event selections	Fit ranges
CDF	$30 < p_T^\ell < 55$ GeV, $\|\eta_\ell\|<1$	$32 < p_T^\ell < 48$ GeV
	$30 < E_T^{miss} < 55$ GeV, $60 < m_T < 100$ GeV	$32 < E_T^{miss} < 48$ GeV
	$u_T < 15$ GeV	$65 < m_T < 90$ GeV
D0	$p_T^\ell > 25$ GeV, $\|\eta_\ell\|<1.05$	$32 < p_T^\ell < 48$ GeV
	$E_T^{miss} > 25$ GeV, $m_T > 50$ GeV	$65 < m_T < 90$ GeV
	$u_T < 15$ GeV	
ATLAS	$p_T^\ell > 30$ GeV, $\|\eta_\ell\|<2.4$	$32 < p_T^\ell < 45$ GeV
	$E_T^{miss} > 30$ GeV, $m_T > 60$ GeV	$66 < m_T < 99$ GeV
	$u_T < 30$ GeV	

Table 3: Event selections and fit ranges for CDF, D0 and ATLAS.

CDF performs measurements in the $W \to e\nu$ and $W \to \mu\nu$ channels, using template fits to the p_T^ℓ, m_T and E_T^{miss} distributions, *i.e* six measurements. D0 uses the p_T^ℓ and m_T distributions in the $W \to e\nu$ channel only. These measurements are performed inclusively in pseudorapidity and summing over W^+ and W^- decays. ATLAS measures W^+ and W^- events separately, as in pp collisions the final state distributions are different for these processes. In addition, the analyzed pseudorapidity range is separated into three categories in the electron channel, and four categories in the muon channel, yielding a total of 28 measurements.

The p_T^ℓ and m_T distributions simulated as above, and obtained after all event selections are compared to the published distributions in Figure 4.

5.3 Quality of the emulated PDF-induced shifts in m_W

The precision of the emulated PDF-induced shifts in the fitted value of m_W is studied using the ATLAS measurement. With 28 measurement categories and 25 CT10nnlo PDF eigensets, a high-statistics comparison between the emulation and the full measurement procedure can be performed.

This comparison is performed in Figure 5, which illustrates the correlation between the published and emulated shifts for CT10nnlo. The shifts are defined as in Section 3.1: $\delta m_W^i = m_W^i - m_W^{ref}$, where the reference set is the CT10nnlo central set, and the variations i are the uncertainty sets.

Analyzing all variations separately (50 shifts for each category), a spread of 3 MeV is found between the published and emulated shifts. When symmetrizing the uncertaintiy variations, i.e. considering only 25 symmetrized shifts, the spread reduces to 1.5 MeV. These numbers are included as a systematic uncertainty associated to the emulation procedure.

6 Results

The methods described above are used to estimate the effect of PDF variations on the existing m_W results by CDF, D0 and ATLAS.

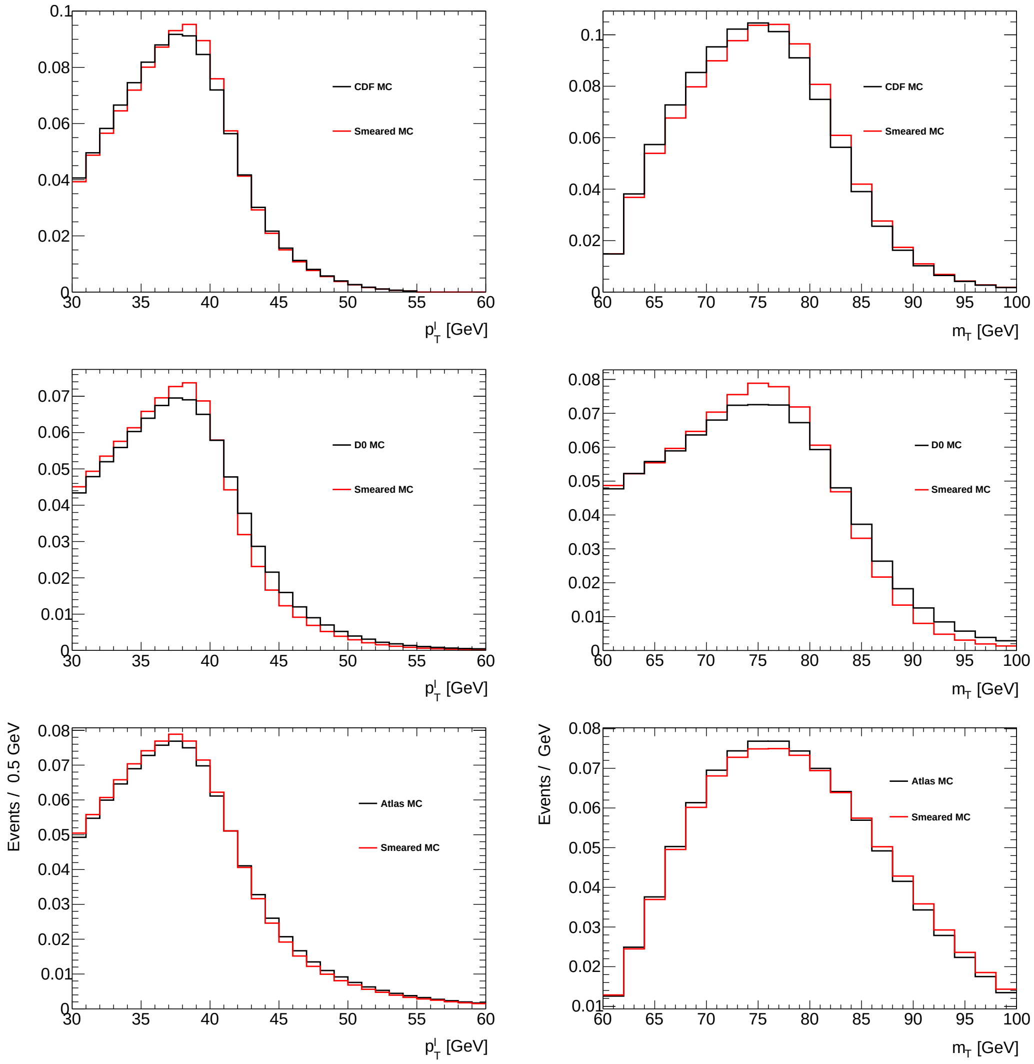

Figure 4: Comparison of the published and simulated p_T^ℓ (lefT) and m_T (right) distributions, for CDF (top), D0 (centre) and ATLAS (bottom).

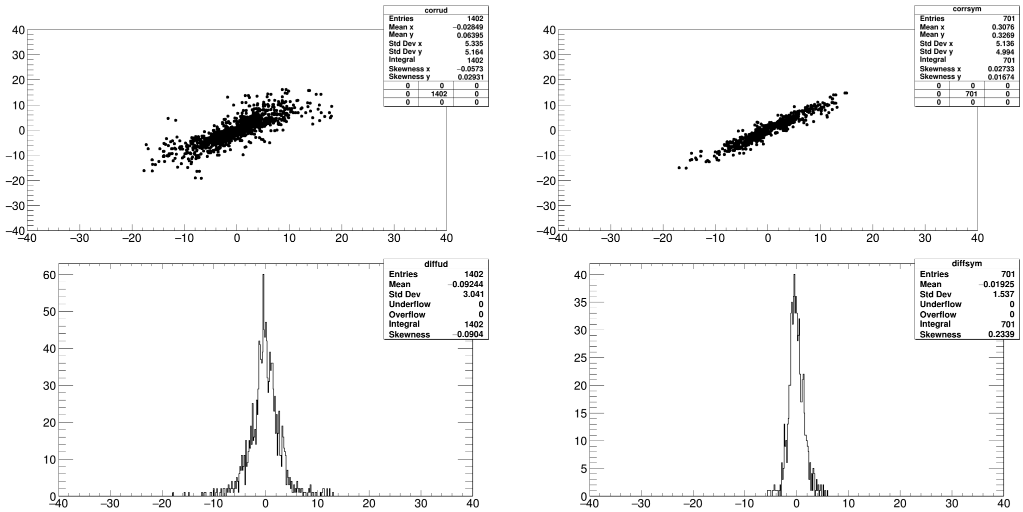

Figure 5: Top : correlation between the published and emulated CT10nnlo PDF shifts, in the MeV, for the ATLAS measurement. Bottom : distribution of the differences between published and emulated shifts. On the left, all uncertainty sets enter the distributions. On the right only symmetrized shifts are considered.

As a first step, the method is validated by reproducing, using the analysis emulation described above, the PDF uncertainty estimates of the corresponding publications. The same techniques are then used to extrapolate, for each experiment, the measurement result to alternate PDFs, and the corresponding uncertainties.

This procedure is applied separately for all measurement results, i.e. six channels for CDF, two for D0, and 28 for ATLAS. The combinations are then performed separately for all experiments, accounting for PDF uncertainty correlations as explaind in Section 3.2.

Fully combined results are then calculated for all considered PDF sets, and a final recommendation is derived.

6.1 Results for CDF

The published CDF results used CTEQ6.6 for the central value with PDF uncertainties estimated using MSTW2008 at 68% CL. The scaling factor between MSTW2008 at 90% CL and MSTW2008 at 68% CL is 2.15 and was found back in the context of this analysis. Extrapolated results for CDF are given in Table 4, and the corresponding PDF uncertainties are given in Table 5. The analysis emulation procedure with MSTW2008 accurately reproduces the published PDF uncertainty.

The combined result is reproduced within 2 MeV. The residual difference is due to the fact that the channel combination is performed using the full PDF uncertainty decomposition (i.e. all PDF uncertainty sets are used seperately in the combination), where the CDF measurement treats the PDF uncertainty as a single, fully correlated nuisance parameter across all channels.

Extrapolating the measurement to different PDF sets yields shifts in the central values smaller than 5 MeV, compared to the published result, for all sets considered here. PDF uncertainties range between 16 MeV for CT10 and 8 MeV for MMHT2014.

Category		CTEQ6.6†	CT10	CT10nnlo	CT14	MSTW2008	MMHT2014
$W \to e\nu$	m_T fit	80 408	80 400	80 408	80 403	80 407	80 402
$W \to e\nu$	p_T^ℓ fit	80 393	80 386	80 391	80 389	80 396	80 391
$W \to e\nu$	E_T^{miss} fit	80 431	80 423	80 431	80 426	80 429	80 425
$W \to \mu\nu$	m_T fit	80 379	80 371	80 379	80 374	80 378	80 373
$W \to \mu\nu$	p_T^ℓ fit	80 348	80 341	80 346	80 344	80 351	80 346
$W \to \mu\nu$	E_T^{miss} fit	80 406	80 398	80 406	80 401	80 404	80 400
Combined (published)		80 387	–	–	–	–	–
Combined (emulated)		80 389	80 382	80 389	80 385	80 388	80 384

Table 4: Fitted values of m_W (MeV) at CDF, for various PDF sets. The PDF set labbelled † is used to define the central value of the published measurement result.

	Published	Emulated					
	CTEQ6.6† MSTW2008§	CTEQ6.6†	CT10	CT10nnlo	CT14	MSTW2008§	MMHT2014
Central value	80 387	80 389	80 382	80 389	80 385	80 388	80 384
Stat.	12	12	12	12	12	12	12
Exp. syst.	10						
QCD, QED	6						
PDF	10	14	16	11	14	10	8
Total	19	22	23	20	21	19	18

Table 5: CDF combination results, for various PDF sets. The first column indicated the published uncertainty table; the next columns indicate the extrapolated central values and PDF uncertainties, calculated consistently with the given PDF set. PDF sets labbelled † and § are used for the published measurement central value and for the PDF uncertainty, respectively.

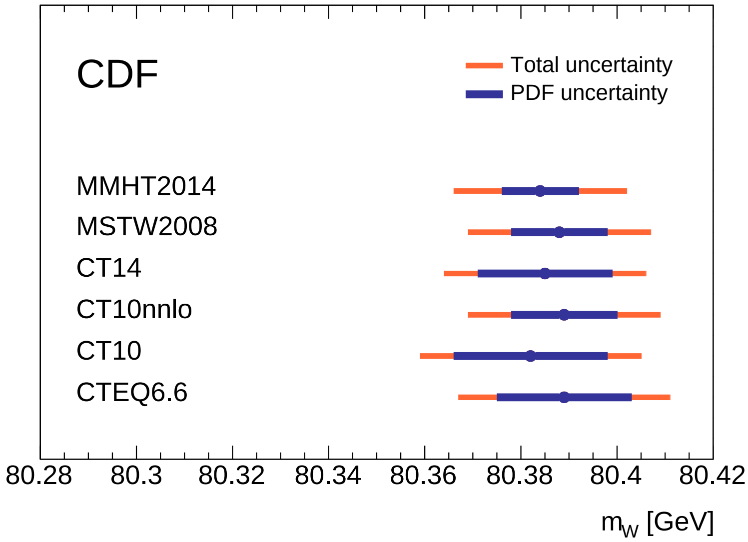

Figure 6: Measured value of m_W in CDF for different PDF sets. The reference PDF set for CDF is CTEQ6.6.

6.2 Results for D0

The published D0 results used CTEQ6.6 PDF set for the central value and CTEQ6.1 for the estimation of PDF uncertainties with a scaling of 1.645 to 68% CL. Extrapolation results for D0 are given in Table 6, and the corresponding PDF uncertainties are given in Table 7.

The analysis emulation yields a CTEQ6.1 PDF uncertainty of 15 MeV, compared to 10 MeV in the D0 publication. This difference remains to be understood. Comparing Tables 7 and 5, it can be noted that the D0 and CDF PDF uncertainties are always close, as expected from the similarity of the measurement conditions and as mentioned in Section 2. The observed difference is therefore likely due to a difference in the physics modelling assumptions rather than the limited accuracy of the paramaterisation of the recoil response and resolution.

The emulated combined result differs from the publication by 3.5 MeV, which is understood as follows. The two channels of the D0 measurement are correlated to 90%; the larger PDF uncertainty found here further increases this correlation.The BLUE combination procedure determines the channel weights such that the resulting uncertainty is minimal; in the limit of full correlation, the weight of the most precise channel tends to 1 and the less precise channel is ignored, even if the difference in precision is very small. In the present case, the m_{T} fit is slightly more precise than the p_{T}^{ℓ} fit, and the combined result tends to that result when the correlation increases. When scaling the PDF uncertainty to reproduce the publication, the published combined value is recovered to better than 1 MeV.

Extrapolating the measurement to different PDF sets yields shifts in the central values smaller than 4 MeV, compared to the published result, for all sets considered here. As for CDF, PDF uncertainties range between 16 MeV for CT10 and 8 MeV for MMHT2014.

6.3 Results for ATLAS

The published ATLAS results used CT10nnlo for both the central value and the estimation of PDF uncertainties with a scaling of 1.645 to 68% CL. Measurement xtrapolation results for ATLAS are given in Table 8, and the corresponding PDF uncertainties are given in Table 9. The analysis emulation procedure reproduces the published PDF uncertainty, and the combined result is reproduced within 1 MeV. As above, this residual difference is mostly due to the influence of the impact of the emulated PDF uncertainties on the channel weights.

Extrapolating the measurement to different PDF sets yields shifts in the central values up to 15 MeV compared to the published result. The larger PDF dependence can be explained an increased PDF model dependence, in a region that is less strongly constrained by the data compared to the Tevatron. PDF uncertainties range from 12 MeV for CT14, down to 5 MeV for MSTW2008.

6.4 Tevatron–LHC combination

This sections presents the complete combination results, including all available results. The procedure, and the full list of considered PDF sets is as above, and the results are shown in Table 10. Figure 9 gives a graphical representation of these results.

TO DO The choice of PDFs considered for the final result is decided following criteria:

Category	CTEQ6.6†	CT10	CT10nnlo	CT14	MSTW2008	MMHT2014
$W \to e\nu$ m_T fit	80 371	80 363	80 371	80 366	80 369	80 365
$W \to e\nu$ p_T^ℓ fit	80 343	80 336	80 341	80 339	80 345	80 340
Combined (published)	80 367	–	–	–	–	–
Combined (emulated)	80 370	80 364	80 370	80 367	80 367	80 363

Table 6: Fitted values of m_W (MeV) at D0, for various PDF sets. The PDF set labbelled † is used to define the central value of the published measurement result.

	Published	Emulated					
	CTEQ6.6†, CTEQ6.1§	CTEQ6.6†	CT10	CT10nnlo	CT14	MSTW2008	MMHT2014
Central value	80 367	80 370	80 364	80 370	80 367	80 367	80 363
Stat.	13	13	13	13	13	13	13
Exp. syst.	18	18	18	18	18	18	18
QCD, QED	7	7	7	7	7	7	7
PDF	11	14	16	11	13	10	8
Total	26	27	28	26	27	25	25

Table 7: D0 combination results (TODO : this is the 4 fb^{-1} result only). The first column indicated the published uncertainty table; the next columns indicate the extrapolated central values and PDF uncertainties, calculated consistently with the given PDF set. PDF sets labbelled † and § are used for the published measurement central value and for the PDF uncertainty, respectively.

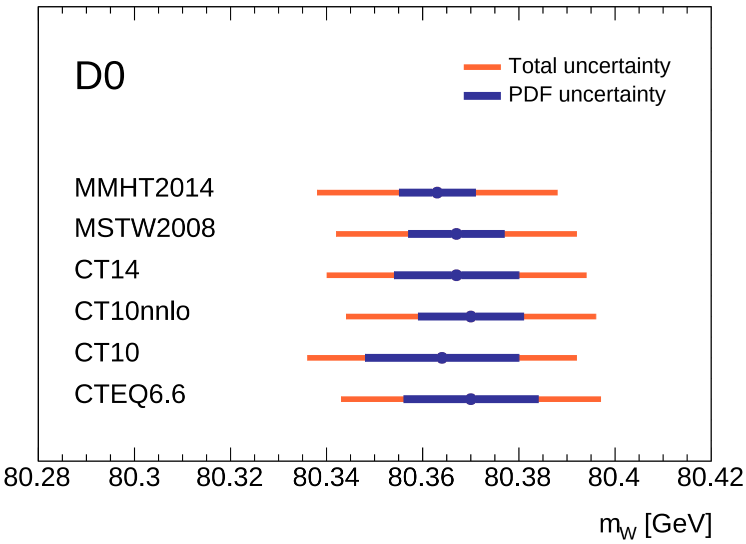

Figure 7: Measured value of m_W in D0 for different PDF sets. The reference PDF set for D0 is CTEQ6.6.

Channel	$\|\eta\|$ range	CT10nnlo†	CT10	CTEQ6.6	CT14	MSTW2008	MMHT2014
m_T fits							
$W^- \to e\nu$	0–0.6	80 416	80 386	80 392	80 405	80 395	80 440
$W^- \to e\nu$	0.6–1.2	80 298	80 280	80 285	80 277	80 287	80 308
$W^- \to e\nu$	1.8–2.4	80 424	80 454	80 437	80 439	80 474	80 418
$W^+ \to e\nu$	0–0.6	80 353	80 321	80 324	80 326	80 318	80 365
$W^+ \to e\nu$	0.6–1.2	80 382	80 352	80 364	80 349	80 340	80 369
$W^+ \to e\nu$	1.8–2.4	80 353	80 341	80 351	80 375	80 291	80 338
$W^- \to \mu\nu$	0–0.8	80 376	80 345	80 352	80 365	80 355	80 400
$W^- \to \mu\nu$	0.8–1.4	80 418	80 400	80 405	80 397	80 407	80 428
$W^- \to \mu\nu$	1.4–2.0	80 380	80 384	80 376	80 367	80 396	80 388
$W^- \to \mu\nu$	2.0–2.4	80 335	80 365	80 347	80 349	80 384	80 328
$W^+ \to \mu\nu$	0–0.8	80 372	80 340	80 342	80 344	80 336	80 383
$W^+ \to \mu\nu$	0.8–1.4	80 355	80 324	80 337	80 321	80 312	80 342
$W^+ \to \mu\nu$	1.4–2.0	80 427	80 403	80 421	80 416	80 374	80 401
$W^+ \to \mu\nu$	2.0–2.4	80 335	80 324	80 333	80 357	80 274	80 320
p_T^ℓ fits							
$W^- \to e\nu$	0–0.6	80 352	80 329	80 333	80 344	80 337	80 370
$W^- \to e\nu$	0.6–1.2	80 310	80 295	80 298	80 295	80 304	80 321
$W^- \to e\nu$	1.8–2.4	80 414	80 435	80 419	80 428	80 455	80 413
$W^+ \to e\nu$	0–0.6	80 337	80 314	80 316	80 318	80 311	80 344
$W^+ \to e\nu$	0.6–1.2	80 346	80 323	80 332	80 322	80 315	80 338
$W^+ \to e\nu$	1.8–2.4	80 345	80 335	80 343	80 363	80 292	80 332
$W^- \to \mu\nu$	0–0.8	80 428	80 406	80 410	80 421	80 414	80 446
$W^- \to \mu\nu$	0.8–1.4	80 396	80 381	80 384	80 381	80 389	80 407
$W^- \to \mu\nu$	1.4–2.0	80 381	80 383	80 376	80 373	80 394	80 390
$W^- \to \mu\nu$	2.0–2.4	80 316	80 337	80 320	80 329	80 357	80 315
$W^+ \to \mu\nu$	0–0.8	80 328	80 305	80 307	80 309	80 302	80 336
$W^+ \to \mu\nu$	0.8–1.4	80 358	80 334	80 344	80 333	80 327	80 349
$W^+ \to \mu\nu$	1.4–2.0	80 447	80 428	80 441	80 439	80 406	80 429
$W^+ \to \mu\nu$	2.0–2.4	80 335	80 324	80 332	80 352	80 281	80 322
Combined (published)		80 370	–	–	–	–	–
Combined (emulated)		80 369	80 355	80 358	80 354	80 353	80 369

Table 8: Fitted values of m_W (MeV) at ATLAS, for various PDF sets. The PDF set labbelled † is used to define the central value of the published measurement result.

	Published	Emulated					
	CT10nnlo†§	CT10nnlo†§	CT10	CTEQ6.6	CT14	MSTW2008	MMHT2014
Central value	80 370	80 369	80 355	80 358	80 354	80 353	80 369
Stat.	7	7	7	7	7	7	7
Exp. syst.	11						
QCD, QED	10						
PDF	9	9	10	8	12	5	9
Total	19	19	19	18	21	17	19

Table 9: ATLAS combination results. The first column indicated the published uncertainty table; the next columns indicate the extrapolated central values and PDF uncertainties, calculated consistently with the given PDF set. Occasional changes between the published and emulated experimental and modelling uncertainties are due to the influence of the PDF uncertainties on the weights of the categories. PDF sets labbelled † and § are used for the published measurement central value and for the PDF uncertainty, respectively.

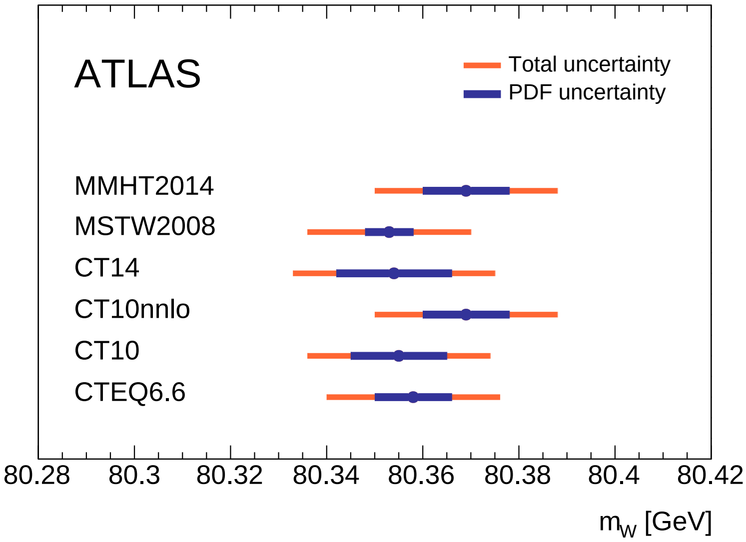

Figure 8: Measured value of m_W in ALTAS for different PDF sets. The reference PDF set for ATLAS is CT10nnlo.

- Consider only the last published set of each PDF fitting group;
- Consider only NNLO PDF fits;
- Consider only sets explicitly providing 68%C.L. uncertainties.

CT14, MMHT2014, NNPDF3.1, ABMP.. survive these criteria.

The final results are shown in Figure 10. The final world average is defined from the flat average between all considered combined results. Assuming full correlation between the different PDF uncertainty estimates, the final PDF uncertainty is defined from the average PDF uncertainty over all sets, as calculated from Table **??**. An addtional uncertainty is counted for for the spread of the m_W central values, defined from half the maximum difference between all fit results.

	CTEQ6.6	CT10	CT10nnlo	CT14	MSTW2008	MMHT2014
Central value	80 367	80 364	80 380	80 373	80 363	80 375
Statistical	6	6	7	7	6	6
Experimental						
Boson p_T						
PDF	9	10	8	9	5	7
Other QCD						
Higher-order EWK						
Total	14	15	14	14	12	13

Table 10: Combination summary

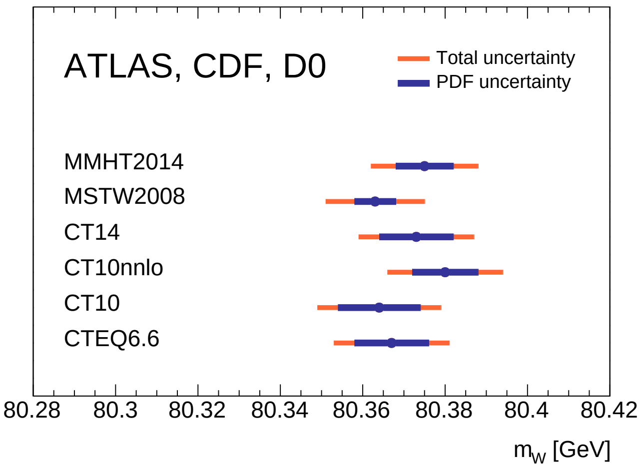

Figure 9: Combined value of m_W for different PDF sets.

7 Conclusion

We have presented a combination of the ATLAS, CDF and D0 measurements of the W-boson mass. These measurements were performed at different moments in time, using different modelling assumptions for W-boson production and decay, using fits to detector-level distributions. The correlations between these measurements are dominated by uncertainties in the PDFs, for which different choices were made. Methods are presented to evaluate the effect of PDF variations on existing measurement results in a realistic way, which allows extrapolating past measurements to any past or present PDF set and eevaluate the corresponding uncertainties. Based on this method, the measurements can be corrected to set of common PDF references, and combined accounting for the partial PDF correlations in a quantitative way. The combined value is

$$m_W = 80XYZ \pm X(\text{exp.}) \pm Y(\text{PDF}) \pm Z(\text{mod.})$$

where the central value has been obtained for PDF set to be defined, conventionally chosen as reference for the combination. Central values for alternate sets are also given.

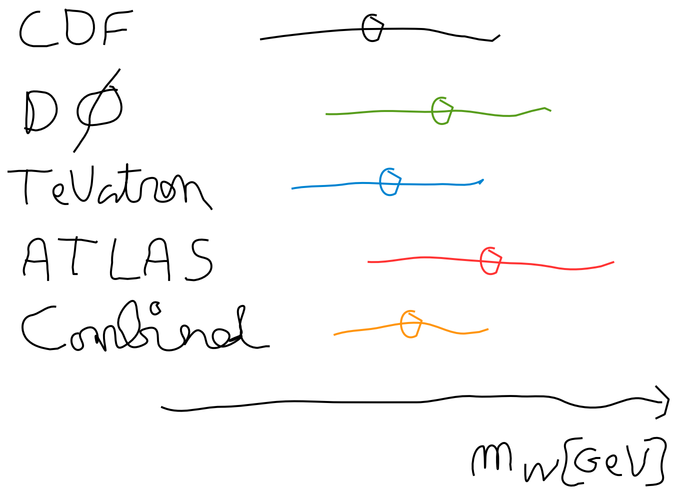

Figure 10: m_W summary plot (CDF, D0, Tevatron, ATLAS and fully combined values). Recommendation for PDF baseline and uncertainty to be decided.

References

[1] T. A. Aaltonen et al., *Precise measurement of the W -boson mass with the Collider Detector at Fermilab*, Phys. Rev. **D89** (2014) 072003, arXiv: 1311.0894 [hep-ex] (cit. on p. 4).

[2] V. M. Abazov et al., *Measurement of the W boson mass with the D0 detector*, Phys. Rev. **D89** (2014) 012005, arXiv: 1310.8628 [hep-ex] (cit. on p. 4).

[3] M. Aaboud et al., *Measurement of the W-boson mass in pp collisions at $\sqrt{s}$ = 7 TeV with the ATLAS detector*, Eur. Phys. J. **C78** (2018) 110, [Erratum: Eur. Phys. J.C78,no.11,898(2018)], arXiv: 1701.07240 [hep-ex] (cit. on p. 4).

[4] F. Landry, R. Brock, P. M. Nadolsky and C. P. Yuan, *Tevatron Run-1 Z boson data and Collins-Soper-Sterman resummation formalism*, Phys. Rev. **D67** (2003) 073016, arXiv: hep-ph/0212159 [hep-ph] (cit. on p. 4).

[5] G. A. Ladinsky and C. P. Yuan, *The Nonperturbative regime in QCD resummation for gauge boson production at hadron colliders*, Phys. Rev. **D50** (1994) R4239, arXiv: hep-ph/9311341 [hep-ph] (cit. on p. 4).

[6] C. Balazs and C. P. Yuan, *Soft gluon effects on lepton pairs at hadron colliders*, Phys. Rev. **D56** (1997) 5558, arXiv: hep-ph/9704258 [hep-ph] (cit. on p. 4).

[7] P. M. Nadolsky et al., *Implications of CTEQ global analysis for collider observables*, Phys. Rev. D **78** (2008) 013004, arXiv: 0802.0007 [hep-ph] (cit. on pp. 4, 10).

[8] P. Nason, *A new method for combining NLO QCD with shower Monte Carlo algorithms*, JHEP **11** (2004) 040, arXiv: hep-ph/0409146 (cit. on pp. 4, 9).

[9] S. Frixione, P. Nason and C. Oleari, *Matching NLO QCD computations with parton shower simulations: the POWHEG method*, JHEP **11** (2007) 070, arXiv: 0709.2092 [hep-ph] (cit. on pp. 4, 9).

[10] S. Alioli, P. Nason, C. Oleari and E. Re, *A general framework for implementing NLO calculations in shower Monte Carlo programs: the POWHEG BOX*, JHEP **06** (2010) 043, arXiv: 1002.2581 [hep-ph] (cit. on pp. 4, 9).

[11] T. Sjöstrand et al., *An Introduction to PYTHIA 8.2*, Comput. Phys. Commun. **191** (2015) 159, arXiv: 1410.3012 [hep-ph] (cit. on pp. 4, 10).

[12] H.-L. Lai, M. Guzzi, J. Huston, Z. Li, P. M. Nadolsky et al., *New parton distributions for collider physics*, Phys. Rev. D **82** (2010) 074024, arXiv: 1007.2241 [hep-ph] (cit. on pp. 4, 10).

[13] J. de Blas et al., *The Global Electroweak and Higgs Fits in the LHC era*, PoS **EPS-HEP2017** (2017) 467, arXiv: 1710.05402 [hep-ph] (cit. on p. 4).

[14] J. Haller et al., *Update of the global electroweak fit and constraints on two-Higgs-doublet models*, Eur. Phys. J. **C78** (2018) 675, arXiv: 1803.01853 [hep-ph] (cit. on p. 4).

[15] M. Tanabashi et al., *Review of Particle Physics*, Phys. Rev. **D98** (2018) 030001 (cit. on p. 4).

[16] T. A. Aaltonen et al., *Combination of CDF and D0 W-Boson Mass Measurements*, Phys. Rev. **D88** (2013) 052018, arXiv: 1307.7627 [hep-ex] (cit. on p. 6).

[17] A. Valassi, *Combining correlated measurements of several different physical quantities*, Nucl. Instrum. Meth. **A500** (2003) 391 (cit. on p. 7).

[18] G. Aad et al., *Measurement of the Z/γ^* boson transverse momentum distribution in pp collisions at $\sqrt{s} = 7$ TeV with the ATLAS detector*, JHEP **09** (2014) 145, arXiv: 1406.3660 [hep-ex] (cit. on p. 8).

[19] L. Barze, G. Montagna, P. Nason, O. Nicrosini and F. Piccinini, *Implementation of electroweak corrections in the POWHEG BOX: single W production*, JHEP **04** (2012) 037, arXiv: 1202.0465 [hep-ph] (cit. on p. 9).

[20] L. Barze et al., *Neutral current Drell-Yan with combined QCD and electroweak corrections in the POWHEG BOX*, Eur. Phys. J. C **73** (2013) 2474, arXiv: 1302.4606 [hep-ph] (cit. on p. 9).

[21] N. Davidson, T. Przedzinski and Z. Was, *PHOTOS Interface in C++: Technical and Physics Documentation*, Comput. Phys. Commun. **199** (2016) 86, arXiv: 1011.0937 [hep-ph] (cit. on p. 9).

[22] D. Stump et al., *Inclusive jet production, parton distributions, and the search for new physics*, JHEP **10** (2003) 046, arXiv: hep-ph/0303013 [hep-ph] (cit. on p. 10).

[23] J. Gao et al., *CT10 next-to-next-to-leading order global analysis of QCD*, Phys. Rev. **D89** (2014) 033009, arXiv: 1302.6246 [hep-ph] (cit. on p. 10).

[24] S. Dulat et al., *New parton distribution functions from a global analysis of quantum chromodynamics*, Phys. Rev. D **93** (2016) 033006, arXiv: 1506.07443 [hep-ph] (cit. on p. 10).

[25] T.-J. Hou et al., *Progress in the CTEQ-TEA NNLO global QCD analysis*, (2019), arXiv: 1908.11394 [hep-ph] (cit. on p. 10).

[26] A. D. Martin, W. J. Stirling, R. S. Thorne, and G. Watt, *Parton distributions for the LHC*, Eur. Phys. J. C **63** (2009) 189, arXiv: 0901.0002 [hep-ph] (cit. on p. 10).

[27] L. A. Harland-Lang, A. D. Martin, P. Motylinski and R. S. Thorne, *Parton distributions in the LHC era: MMHT 2014 PDFs*, Eur. Phys. J. C **75** (2015) 204, arXiv: 1412.3989 [hep-ph] (cit. on p. 10).

[28] R. D. Ball et al., *Parton distributions from high-precision collider data*, Eur. Phys. J. C **77** (2017) 663, arXiv: 1706.00428 [hep-ph] (cit. on p. 10).

[29] S. Alekhin, J. Blümlein, S. Moch and R. Placakyte, *Parton distribution functions, α_s, and heavy-quark masses for LHC Run II*, Phys. Rev. D **96** (2017) 014011, arXiv: 1701.05838 [hep-ph] (cit. on p. 10).

[30] A. Accardi, L. T. Brady, W. Melnitchouk, J. F. Owens and N. Sato, *Constraints on large-x parton distributions from new weak boson production and deep-inelastic scattering data*, Phys. Rev. D **93** (2016) 114017, arXiv: 1602.03154 [hep-ph] (cit. on p. 10).

[31] ATLAS Collaboration, *Measurement of the Z/γ^* boson transverse momentum distribution in pp collisions at $\sqrt{s} = 7$ TeV with the ATLAS detector*, JHEP **09** (2014) 145, arXiv: 1406.3660 [hep-ex] (cit. on p. 10).

The supporting notes for the analysis should also contain a list of contributors. This information should usually be included in `mydocument-metadata.tex`. The list should be printed either here or before the Table of Contents.

List of contributions

Appendices

A p_{T}^{Z}-constrained final state distributions for CTEQ6.6, CT14, MMHT2014 and NNPDF3.1

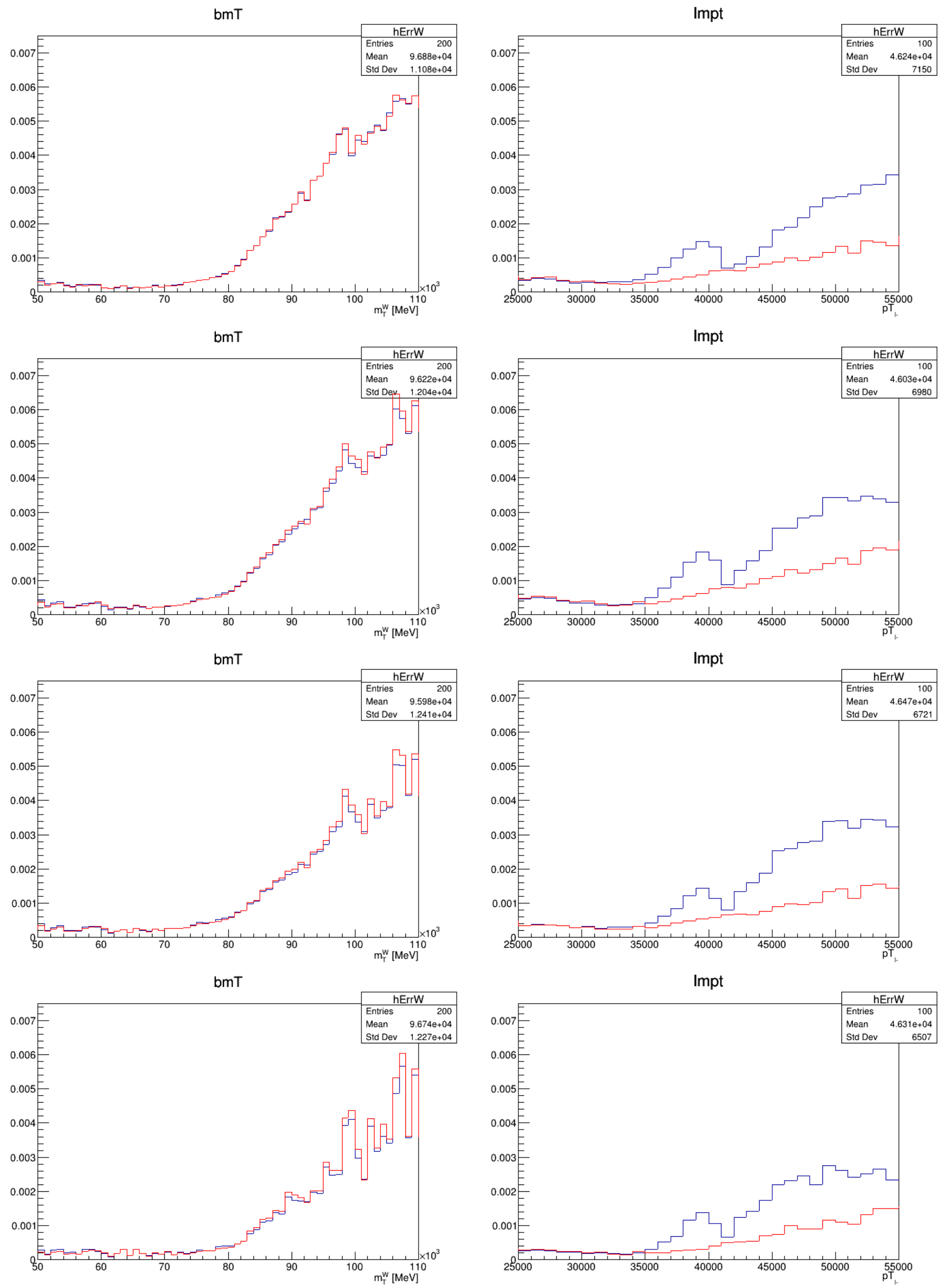

Figure 11: Effect of the pTZ constraint on the generator-level transverse mass (left) and lepton p_T (right) distributions, for CTEQ6.6, CT10, CT14 and MMHT2014.